Control Engineering Practice 58 (2017) 107–116

Contents lists available at ScienceDirect

Control Engineering Practice

journal homepage: www.elsevier.com/locate/conengprac

Multimode combustion in a mild hybrid electric vehicle. Part 2: Three-way catalyst considerations

Sandro Nüesch*, Anna G. Stefanopoulou

Department of Mechanical Engineering, University of Michigan, 2350 Hayward, Ann Arbor, MI 48109, USA

ARTICLE INFO

Keywords:
Homogeneous charge compression ignition (HCCI) combustion
Mild HEV
Internal combustion engines
Powertrain control
Combustion mode switch
Supervisory control
Three-way catalyst

ABSTRACT

This is the second of a two-part study that discusses multimode combustion in a mild hybrid electric vehicle. Homogeneous charge compression ignition (HCCI) combustion oxidizes the oxygen storage capacity (OSC) of the three-way catalyst (TWC), thereby removing the TWC's ability to convert NOx under lean conditions. Despite prolonged operation in HCCI mode, enabled by the electric motor, the depletion of the OSC causes significant penalties in fuel economy and the amounts of tailpipe NOx are substantial. Counter-intuitively, it is seen that decreasing the sizes of both HCCI regime and OSC results in reduced tailpipe NOx while maintaining fuel economy benefits.

1. Introduction

This is the second part of a two-part simulation study on multimode combustion in a hybrid electric vehicle (HEV). In particular it is focused on a SI/HCCI engine integrated in a 48 V-like mild HEV. In the previous paper (Part 1, (Nüesch & Stefanopoulou, 2016)) four different supervisory control strategies are compared in terms of fuel economy. A finite state combustion mode switch model, presented in Nüesch, Gorzelic, Jiang, Sterniak, and Stefanopoulou (2016), is used to describe mode switch dynamics and fuel penalties during the switching. The optimal torque-split between engine and integrated starter-generator (ISG) is based on an equivalent consumption minimization strategy (ECMS) with four supervisors responsible for deciding, when to switch between SI and HCCI mode. It was seen that during the FTP75 drive cycle the relative fuel economy benefit of multimode over SI-only combustion is significantly greater in case of the mild HEV compared to the conventional vehicle. This suggests a great synergy between the ISG's torque assist and HCCI's high efficiency. Further it was concluded that, especially during the HWFET drive cycle, it is necessary to integrate the battery's state-of-charge (SOC) into the mode switching decision. The associated optimal strategy would switch out of HCCI as soon as a low SOC is reached and would not allow to further extend the residence time in the mode.

However, besides the dynamics and penalties connected to the combustion mode switch it is important to also consider the interaction of the multimode engine with the aftertreatment system in both, drive cycle simulations and supervisory control. Aftertreatment systems for lean engines are generally very expensive. HCCI's low engine-out NO_x offers the potential to use a relatively inexpensive three-way catalytic converter (TWC). In stoichiometric SI the TWC reduces all emissions as usual. In lean HCCI the TWC would still be able to reduce *HC* and *CO* while break-through of relatively low NO_x might be acceptable. This architecture, however, has two drawbacks. First, the low exhaust temperatures of HCCI might lead to cool-down of the TWC, thereby resulting in low conversion efficiencies for *CO* and *HC*. This problem has been addressed in a control strategy by Kulzer, Sauer, Karrelmeyer, and Fischer (2007). Second, lean HCCI operation results in filling of the TWC's oxygen storage capacity (OSC). In SI operation the OSC represents a buffer for deviations from stoichiometry. To maintain high conversion efficiencies in SI, rich operation is required to deplete the OSC, thereby resulting in large fuel penalties. These penalties have the potential to significantly reduce HCCI's original efficiency benefits, as shown in Nüesch, Jiang, Sterniak, and Stefanopoulou (2015). Experimental results on the OSC dynamics during combustion mode switching have been presented in Chen, Sima, Lin, Sterniak, and Bohac (2015).

Abbreviation: AFR, air-fuel ratio; ECMS, equivalent consumption minimization strategy; ECU, engine control unit; HCCI, homogeneous charge compression ignition; HEV, hybrid electric vehicle; ISG, integrated starter-generator; OSC, oxygen storage capacity; SI, spark-ignited; SOC, state-of-charge; TWC, three-way catalytic converter; *Bsl*, baseline; *Opt*, optimal; *ph*, phase; *sw*, switch; *OC*, open-circuit; *des*, desired; *al*, auxiliary load; *cl*, clutch; *sat*, saturated; *act*, actual; *cat*, catalyst; *amb*, ambient; *cond*, conduction; *conv*, convection; *geo*, geometric; *ri*, rich; *Sml*, small; *Str*, stratified

* Corresponding author.
E-mail addresses: snuesch@umich.edu (S. Nüesch), annastef@umich.edu (A.G. Stefanopoulou).

http://dx.doi.org/10.1016/j.conengprac.2016.10.007
Received 14 December 2015; Received in revised form 2 October 2016; Accepted 17 October 2016
Available online 28 October 2016
0967-0661/

In this paper the mild HEV model with SI/HCCI multimode engine from Nüesch and Stefanopoulou (2016) is extended in two ways, first with an engine exhaust temperature model by Gao, Conklin, Daw, and Chakravarthy (2010) to describe the TWC's temperature and second with a TWC model, described in Nüesch et al. (2015) to simulate the OSC dynamics. This simulation is used to analyze drive cycle fuel economy as well as tailpipe NO_x emissions of the system. Further, two case studies are presented, outlining the influence of different hardware design on fuel economy and NO_x emissions.

Closely related research has been presented in Nüesch et al. (2016). This article expands on that work by providing more details on the TWC model and its validation with experiments. Further a small case study is added which approximates conditions during a stratified HCCI-SI mode switch. This paper is organized as follows: In Section 2 the TWC model is presented. In Section 3 the applied supervisory control strategies are summarized. The drive cycle results are discussed in Section 4, followed by the case studies in Section 5.

2. Vehicle model

The longitudinal vehicle model was parameterized for a stock Cadillac CTS 2009 with 6-speed manual transmission and a curb mass of 1700 kg. It is described in detail in Nüesch and Stefanopoulou (2016). Chassis dynamometer data was used to validate the vehicle model qualitatively, e.g., in terms of load profile, and quantitatively, e.g., in terms of drive cycle fuel economy. The differences between measured and simulated fuel economy were: FTP75 (+0.5%), HWFET (−9.4%), and US06 (+4.5%). More details on its validation is provided in Nüesch (2015). In the following section it is focused on required additions to integrate the model of the TWC aftertreatment system.

2.1. Aftertreatment system

A central aspect of the supervisory control of a multimode combustion engine is its interaction with the aftertreatment system. The system used in this article was parameterized based on two TWCs in series. The first TWC is based on two bricks which are located in a single can. Its two substrates are based on *Pd* and *PdRh*. The second TWC is located underfloor and is based on a *PdRh* substrate. The TWCs offer generous OSC based on CeO_2-ZrO_2. More on the experimental setup and the applied hardware can be found in Chen et al. (2015). The close coupled TWC is used for control purposes. Its inputs and outputs are shown in Fig. 1. Its volume V_{cat} is 1.29 L and its gas volume fraction ϵ_{cat} is 0.8. As can be seen, relative AFR is measure up- and downstream of the first TWC using a wide-range and a switching-type λ-sensors, respectively. The measurements are used to estimate the relative OSC $\widetilde{\Theta}$. More on this estimation strategy can be found in Nüesch et al. (2015).

2.1.1. Oxygen storage

The excess O_2 during lean HCCI operation leads to saturation of the TWC's OSC. With a full OSC the TWC is unable to reduce the engine-out NO_x when facing lean exhaust gas. This may be acceptable under certain HCCI conditions. However, it cannot be tolerated in SI mode, since AFR-control does not always guarantee operation at exact stoichiometry, especially during transients. Therefore, a full OSC needs to be depleted by operating the engine rich as soon as SI combustion is reached. In this paper a phenomenological OSC model by Brandt, Wang, and Grizzle (2010) is applied. The model is based on a saturated integrator with a single state describing the current relative OSC Θ. The implementation and parameterization of the model as well as strategies to deplete the OSC are described in Nüesch et al. (2015). For the convenience of the reader the equation describing the oxygen storage estimator is repeated here:

$$\dot{\widetilde{\Theta}} = \frac{0.23 \cdot \dot{m}_{exh}}{\widetilde{C}_{0,1}} \cdot \left(1 - \frac{1}{\lambda_{exh}}\right) \tag{1}$$

with $\dot{m}_{exh}$ and λ_{exh} mass flow and relative AFR of the exhaust, respectively, and $\widetilde{C}_{0,1}$ the estimated OSC. Model parameters, e.g., $\widetilde{C}_{0,1} = 0.7$, were identified in Nüesch et al. (2015) using lean-rich cycling experiments. As can be seen, the applied oxygen storage model neglects the influence of temperature. More detailed models oxygen storage dynamics, e.g., the control-oriented model by Kibitz, Onder, and Guzzella (2012), take into account reaction rates, rather than simplifying the process using an integrator. Temperature directly affects those reaction rates through, as shown in Arrhenius relationships.

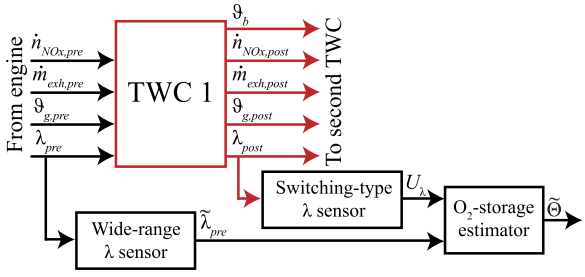

Fig. 1. Block diagram with inputs and outputs of the close coupled TWC.

2.1.2. Brick temperature

The second way HCCI combustion is able to affect the TWC is its low exhaust temperature. As discussed in Kulzer et al. (2007) prolonged residence in HCCI can lead to decrease in TWC brick temperature, which in turn leads to a reduction in its conversion efficiency for *CO* and *HC*. Therefore the TWC's brick temperature needs to be monitored to initiate a switch back to SI combustion.

For many reasons accurate modeling of TWCs is a demanding task. Various aspects need to be taken into account, e.g., two distinct phases, temperature, mass, chemical composition, temporal and two spatial dimensions. In general, the temperature dynamics of the gas phase are significantly faster than the ones in the solid phase. Solving such coupled differential equations is not trivial. Depending on the application, TWC need to be simplified to allow computation in a reasonable amount of time. A simplified TWC temperature model provided by Guzzella and Onder (2010) distinguishes between the temperature of the gas phase ϑ_g and the brick temperature ϑ_b. However, similar to Sanketi and Hedrick (2005), Kum, Peng, and Kucknor (2011), the model applied in this article has been even further reduced to 0D to allow for fast computation when simulating entire drive cycles. It needs to mentioned that this also significantly reduces the accuracy of the model.

$$\epsilon_{cat} V_{cat} \rho_{exh} c_{v,g} \frac{d}{dt}\vartheta_g = c_{p,g} \dot{m}_{exh} (\vartheta_{pre} - \vartheta_g) - \dot{Q}_{gb} \tag{2}$$

$$m_{cat} c_b \frac{d}{dt}\vartheta_b = \dot{Q}_{gb} + \dot{Q}_R - \dot{Q}_{loss}. \tag{3}$$

Parameters are TWC mass and specific heat capacity m_{cat} and c_b, respectively. ϵ_{cat} denotes the volume fraction of the TWC filled with exhaust gas, V_{cat} the volume of the TWC, c_b the specific heat capacity of the solid phase, and m_{cat} the mass of the TWC. Inputs to the model are exhaust gas mass flow and temperature, ϑ_{pre}, $\dot{m}_{exh}$, respectively. Exhaust gas density and specific heat capacities ρ_{exh}, $c_{v,g}$, and $c_{p,g}$, respectively, are calculated as functions of temperature and composition, approximated as described by Heywood (1988, chapter 4). $\dot{Q}_{gb}$ and $\dot{Q}_{loss}$ describe heat transfers between gas-phase and brick as well as brick and environment, respectively:

$$\dot{Q}_{gb} = \alpha_{cat} A_{geo} V_{cat} (\vartheta_g - \vartheta_b) \tag{4}$$

$$\dot{Q}_{loss} = A_{cat} U_{cat} (\vartheta_b - \vartheta_{amb}) \tag{5}$$

with α_{cat} and U_{cat} heat transfer coefficients, A_{cat} the TWC surface area, and A_{geo} [m^2/m^3] the specific geometric catalytic surface, defined as $A_{geo} = 4\sqrt{\epsilon_{cat} \cdot \frac{cpsi}{0.0254^2}}$ in Kiwitz (2012). The heat losses to the environment are based on conduction and free convection coefficients, h_{cond} and h_{conv}, respectively, with $U_{cat} = (h_{cond}^{-1} + h_{conv}^{-1})^{-1}$.

Similar to Shaw, Fischer, and Hedrick (2002) the model is based on the overall chemical reactions:

$$NO + CO \rightarrow \frac{1}{2}N_2 + CO_2 \tag{6}$$

$$CO + \frac{1}{2}O_2 \rightarrow CO_2 \tag{7}$$

$$H_aC_b + (b + \frac{a}{4})O_2 \rightarrow bCO_2 + \frac{a}{2}H_2O \tag{8}$$

with HC modeled as 86% propene and 14% methane. This is a simplifying assumption, since the oxidation rates of hydrocarbons, especially methane, vary strongly with composition.

The produced heat of the chemical reactions $\dot{Q}_r$ then follows as

$$\dot{Q}_r = \sum_k (\dot{n}_{post,k} - \dot{n}_{pre,k}) \cdot \Delta H_{r,k}(\vartheta_b), \quad k = \{NO, CO, HC\} \tag{9}$$

with incoming and outgoing molar flow of the species $\dot{n}_{pre,k}$ and $\dot{n}_{post,k}$, respectively, and associated heat of reaction ΔH_r. Similar to Shaw et al. (2002) the conversion efficiencies of the three overall reactions as a function of relative AFR were used to approximate the incoming and outgoing exhaust gas composition. This results in the following terms for the reaction enthalpies:

$$\Delta h_{r,1} = h_{NO} + h_{CO} - \left(\frac{1}{2}h_{N_2} + h_{CO_2}\right) \tag{10}$$

$$\Delta h_{r,2} = h_{CO} + \frac{1}{2}h_{O_2} - h_{CO_2} \tag{11}$$

$$\Delta h_{r,3,a} = h_{C_3H_6} + 4.5h_{O_2} - (3h_{CO_2} + 3h_{H_2O}) \tag{12}$$

$$\Delta h_{r,3,b} = h_{CH_4} + 2h_{O_2} - (h_{CO_2} + 2h_{H_2O}). \tag{13}$$

Using the TWC's conversion efficiencies, the reaction rates of the three reactions are approximated, resulting in the total heat produced $\dot{Q}_r$:

$$\dot{Q}_{r,1} = \Delta h_{r,1} \cdot \eta_{NO_x} \cdot \dot{n}_{NO_x,in} \tag{14}$$

$$\dot{Q}_{r,2} = \Delta h_{r,2} \cdot (\eta_{CO} \cdot \dot{n}_{CO,in} - \eta_{NO_x} \cdot \dot{n}_{NO_x,in}) \tag{15}$$

$$\dot{Q}_{r,3} = (0.86 \cdot \Delta h_{r,3,a} + 0.14 \cdot \Delta h_{r,3,b}) \cdot \eta_{HC} \cdot \dot{n}_{HC,in} \tag{16}$$

$$\dot{Q}_r = \dot{Q}_{r,1} + \dot{Q}_{r,2} + \dot{Q}_{r,3}. \tag{17}$$

The values for m_{cat} and c_b are based on assumptions and examples in literature while steady-state data was used to determine h_{cond} and α_{cat}. The parameters of the TWC temperature model for both TWC bricks are listed in Table 1. For the enthalpy parameters, general values available in literature were used. This TWC temperature model is very simplified. Steady-state temperature measurement data was obtained

Table 1
TWC temperature model parameters.

Name	Symbol	TWC 1	TWC 2
Specific geometric catalytic surface	A_{geo}	$3.45 \cdot 10^3$ m^2/m^3	$2.82 \cdot 10^3$ m^2/m^3
TWC volume	V_{cat}	$1.29 \cdot 10^{-3}$ m^3	$1.05 \cdot 10^{-3}$ m^3
Gas volume fraction	ϵ_{cat}	0.8	
Catalyst mass	m_{cat}	0.45 kg	0.3 kg
Specific heat capacity of TWC	c_b	800 J/kg K	
Heat transfer gas - solid	α_{cat}	140 W/m^{2}K	
Outer surface area of TWC	A_{cat}	0.0492 m^2	0.0492 m^2
Heat conductivity of TWC wall	h_{cond}	0.5 W/m^{2}K	

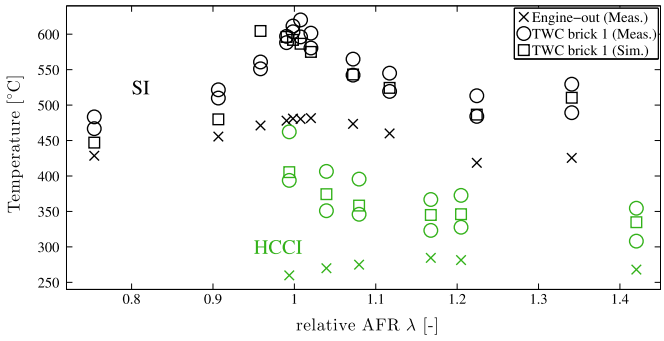

Fig. 2. Steady-state experiments and simulation of TWC brick 1 temperature for SI (black) and HCCI (green) combustion, over sweeps of relative AFR from rich to lean conditions. Engine-out exhaust gas temperature (cross), brick temperature measurements and (square) and simulations (circle). The brick temperature is measured at two locations. (For interpretation of the references to color in this figure, the reader is referred to the web version of this article.)

at various AFR conditions and in both combustion modes and compared to the TWC temperature model results, shown in Fig. 2. Input to the model was the measured engine-out exhaust gas temperature. The brick temperature of the first TWC was measured at two locations. As can be seen, the model under estimates the temperature at rich SI conditions. However, at stoichiometric and at lean conditions in both combustion modes the estimated temperature lies between the two measurements and displays acceptable steady-state-accuracy. Additional validation data under dynamic conditions can be found in Nüesch (2015), where the model was compared to temperature data from chassis dynamometer experiments. When simulating the cold start of the FTP75 drive cycle, ambient temperature was chosen as initial condition of the TWC.

2.1.3. Oxygen storage depletion constraints

The variable R_{TWC} is used to describe constraints posed by the TWC. If the OSC is estimated to be full, rich SI operation is demanded. On the other hand, if the catalyst brick temperature ϑ_b drops below a threshold ϑ_{min}, only stoichiometric SI mode is allowed:

$$R_{TWC} = \begin{cases} \text{rich SI} & \widetilde{\Theta} \geq 0.9 \quad \text{and} \quad M \in (1-3,\ 10-14) \\ \text{stoich. SI} & \vartheta_b < \vartheta_{min} \\ \text{HCCI} & \text{else.} \end{cases} \tag{18}$$

As can be seen, the implemented OSC-depletion strategy allows operation in HCCI with full OSC and tolerates the associated breakthrough in NO_x. Rich SI is only demanded once high lift conditions are reached during the HCCI-SI mode switch. This strategy as well as an alternative, in which the OSC is never allowed to be full, are described in Nüesch et al. (2015).

2.2. Engine

The engine considered is a turbocharged 2.0 L I4 multimode engine. Its model is based on steady-state data for SI and HCCI combustion of fuel, emissions, and exhaust temperature (Nüesch et al., 2016). The maps for HCCI engine-out NO_x and temperature are shown in Fig. 3. Included are two exemplary operating conditions in SI combustion. As can be seen those SI conditions exhibit significantly higher exhaust temperatures and engine-out NO_x than the HCCI operating points nearby. The associated HCCI efficiency maps can be found in Nüesch & Stefanopoulou (2016).

The maps of the two combustion modes are connected by the mode switch model, described in Nüesch et al. (), and implemented within the dynamic vehicle simulation as in Nüesch and Stefanopoulou (2015). A methodology presented by Gao et al. (2010) was implemented to capture engine exhaust temperature dynamics during transients and cold start. A period of approx. 5 min is required to warm up the

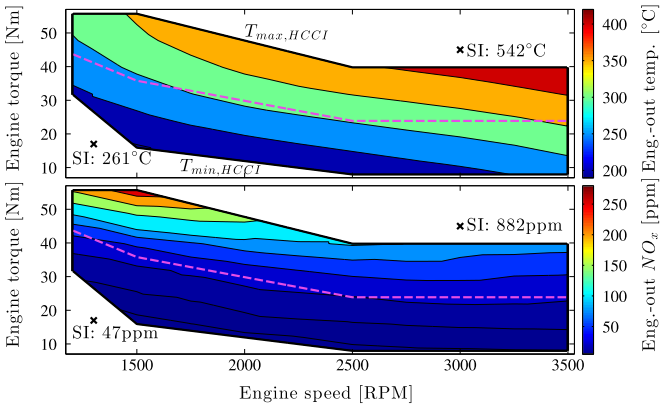

Fig. 3. Steady-state data of the 2.0 L multimode engine in HCCI mode. Top: Engine-out temperature. Bottom: Engine-out NO_x. Dashed line represents center torque in HCCI regime, used in Case Study 2. Black cross: Exemplary SI conditions. See Fig. 2 of Nüesch & Stefanopoulou (2016) for the fuel efficiency.

engine at the beginning of the FTP75 drive cycle, during which the engine is unable to switch to HCCI combustion.

2.2.1. Combustion mode switch

The combustion mode switch model used in Nüesch and Stefanopoulou (2016) is extended here with two additional finite states $M \in (13, 14)$ to implement depletion of the OSC immediately after the switch back to SI. The modified state machine is shown in Fig. 4. Besides parameters for fuel penalty d_M and residence time Δt_M each intermediate state M also exhibits relative air-fuel ratio (AFR) λ_M and engine-out NO_x emissions $NO_{x,M}$. The parameters of the finite-state model can be found in Table 2. Fuel penalties, residence times, and AFR are based on closed-loop SI-HCCI and HCCI-SI mode switch experiments. More on determining the mode switch fuel penalties can be found in Gorzelic (2015). As a simplification it is assumed that NO_x during the switch is mainly determined by the steady-state map of the associated combustion mode and that no spikes in NO_x occur.

The two main control inputs to the combustion mode switch model u_{ph} and u_{sw} determine when to phase the valves and when to switch the cams, respectively. They are described in detail in Nüesch and Stefanopoulou (2016). An additional, third control input u_{ri} is introduced, responsible for rich operation in SI mode. If $u_{ri} = 1$ the engine is operated at a rich relative AFR of $\lambda = 0.9$, instead of $u_{ri} = 0$ when a stoichiometric mixture of fuel and air is used.

Table 2
Finite state mode switch model parameters for SI/HCCI cam switch strategy. Fuel penalty (FP) is relative to nominal baseline fuel flow in SI or HCCI. Residence times are in seconds or engine cycles. In M=2 the duration is interpolated as a function of current engine load, with shorter durations at the top and longer durations at the bottom HCCI load limit. λ_{HCCI}, $NO_{x,SI}$, and $NO_{x,HCCI}$ are based on steady-state maps of associated nominal modes at current load/speed condition.

State M		FP d_M	Δt_M	λ_M	$NO_{x,M}$
SI-HCCI	2 (SI)	6%	0.24–0.42 s	1	$NO_{x,SI}$
	3 (SI)	0%	1 cyc	1	$NO_{x,SI}$
	4 (HCCI)	14%	1 cyc	$0.6\lambda_{HCCI} + 0.4$	$NO_{x,HCCI}$
	5 (HCCI)	3%	2 cyc	λ_{HCCI}	$NO_{x,HCCI}$
	6 (HCCI)	0%	3 cyc	λ_{HCCI}	$NO_{x,HCCI}$
HCCI-SI	8 (HCCI)	4%	0.25 s	λ_{HCCI}	$NO_{x,HCCI}$
	9 (HCCI)	14%	1 cyc	$0.5\lambda_{HCCI} + 0.5$	$0.05NO_{x,SI}$
	10 (SI)	68%	1 cyc	0.9	$0.5NO_{x,SI}$
	11 (SI)	60%	1 cyc	0.9	$0.5NO_{x,SI}$
	12 (SI)	5%	0.25 s	1	$NO_{x,SI}$
	13 (SI)	16%	0.25 s	0.9	$0.5NO_{x,SI}$
	14 (SI)	11%	–	0.9	$0.63NO_{x,SI}$

2.2.2. Mode switch scheduling

Exemplary SI-HCCI and HCCI-SI mode switches during a drive cycle simulation are shown in Figs. 5 and 6, respectively. Note that the figure depicts the same situation as the corresponding plots in Nüesch and Stefanopoulou (2016). However, here the HCCI-SI mode switch includes depletion of the OSC and the trajectories for AFR and engine-out NO_x.

The supervisory control strategies, described in Nüesch and Stefanopoulou (2016), result in requested operating regimes, denoted R_{act}, R_{in}, $R_{out,1}$, and $R_{out,2}$. The additional variable R_{TWC} is used to describe the TWC constraints and introduced below. These constraints require the following minor adjustments to the mode switch scheduling depending on current combustion mode M:

- In SI, M=1, the state of the TWC, represented by R_{TWC}, needs to

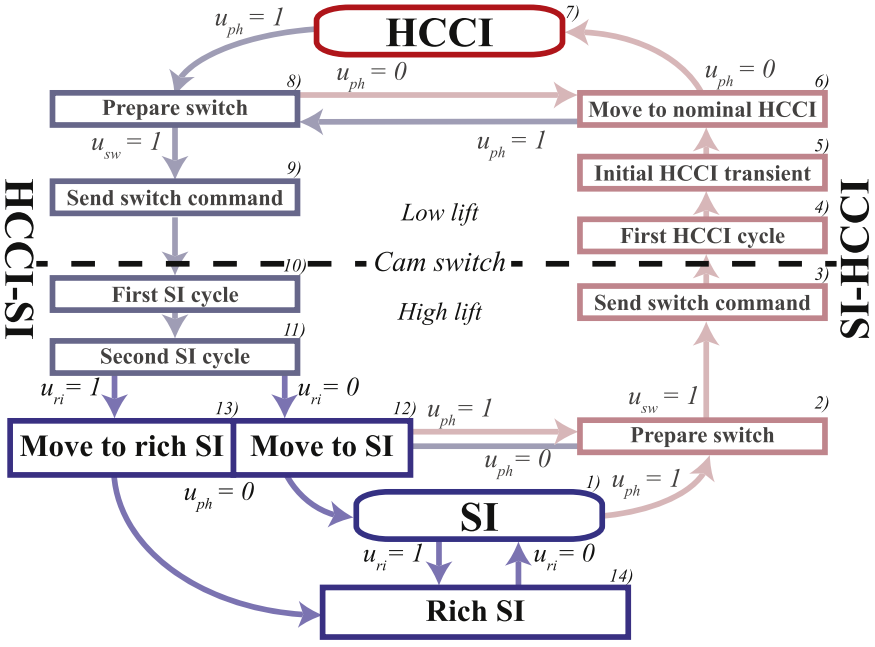

Fig. 4. Combustion mode switch model based on finite-state machine. The dashed line represents the cam switch.

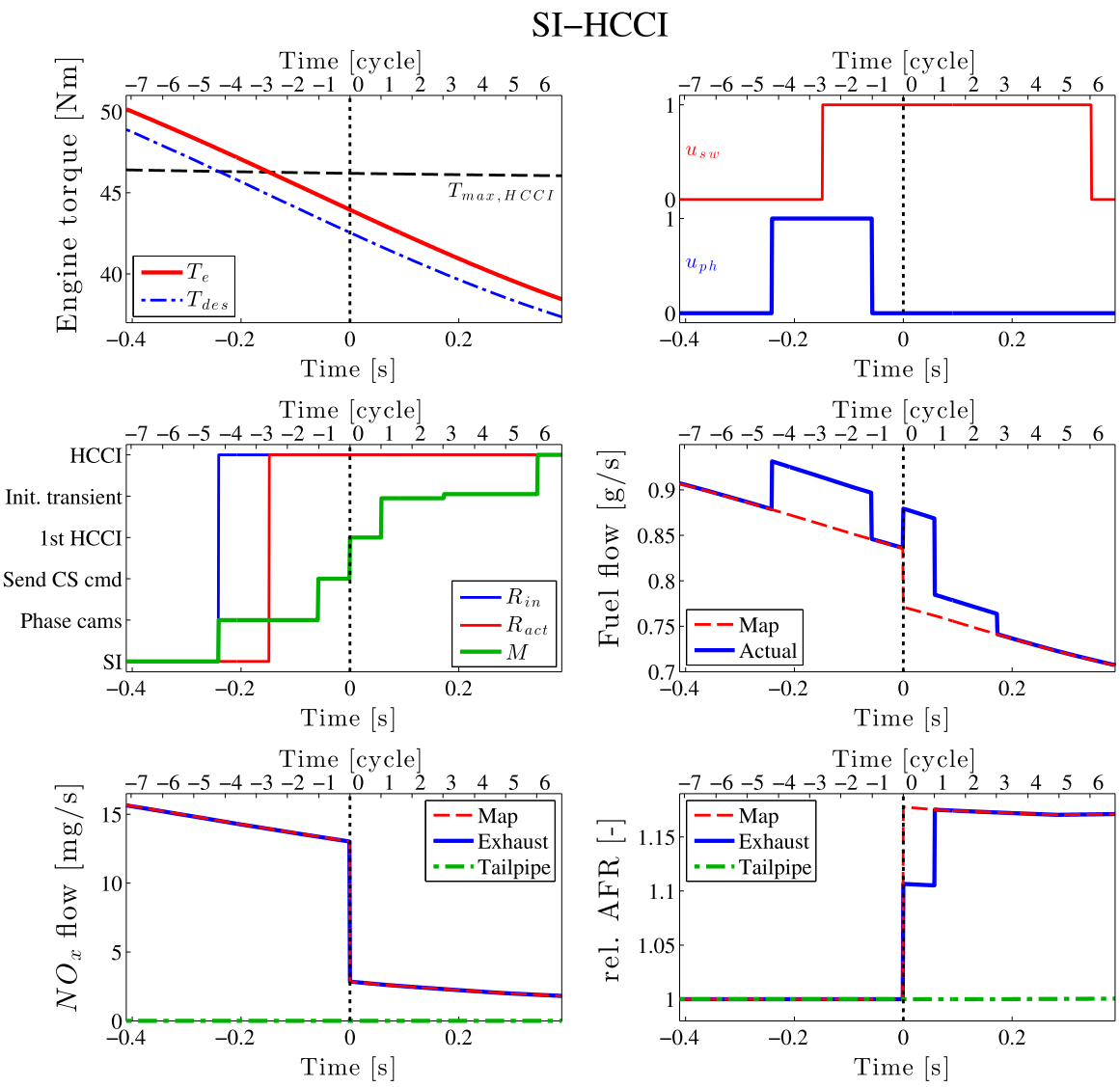

Fig. 5. Exemplary combustion mode switches from SI to HCCI during simulation of the conventional vehicle with supervisory strategy *Bsl* during the FTP75 drive cycle. The variables are plotted over time (bottom-axis) and engine cycles (top-axis). Engine speed is 2500 RPM. The finite states $M \in (5, 6)$ are both summarized as *Init. transient*.

allow a mode switch to HCCI. Alternatively rich SI operation can be requested as well:

$$u_{ph} = \begin{cases} 1 & R_{in} = \text{HCCI and } R_{TWC} = \text{HCCI} \\ 0 & \text{else} \end{cases} \tag{19}$$

$$u_{ri} = \begin{cases} 1 & R_{TWC} = \text{rich SI} \\ 0 & \text{else.} \end{cases} \tag{20}$$

- During the SI-HCCI mode switch, $M \in (2-6)$, as well as in nominal HCCI mode, M=7, the TWC constraints are included to initiate a mode switch back to SI, e.g., in case of a drop in TWC temperature:

$$u_{ph} = \begin{cases} 0 & (R_{act} = \text{SI and} R_{in} = \text{SI}) \ldots \\ & \text{or} R_{TWC} \neq \text{HCCI} \\ 1 & \text{else.} \end{cases} \tag{21}$$

- At the beginning of the HCCI-SI switch, M=8, the cams remain in prepared conditions as long as either both $R_{out,1}$ and $R_{out,2}$ or R_{TWC} demand SI mode:

$$u_{ph} = \begin{cases} 0 & R_{out,1} = \text{HCCI and } R_{out,2} = \text{HCCI} \ldots \\ & \text{and } R_{TWC} = \text{HCCI} \\ 1 & \text{else} \end{cases} \tag{22}$$

$$u_{sw} = \begin{cases} 1 & (R_{out,1} = \text{SI and } R_{out,2} = \text{SI}) \ldots \\ & \text{or } R_{TWC} \neq \text{HCCI} \\ 0 & \text{else.} \end{cases} \tag{23}$$

- As mentioned in Nüesch and Stefanopoulou (2016), upon entering high lift conditions in $M \in (10, 11)$, the engine will be operated rich to enable the TWC to reduce the increased levels NO_x, as shown in Fig. 6 at $t > 0$ s. This results in the relatively high fuel efficiency penalties. After the first two SI-cycles, depending on R_{TWC}, it is decided to either continue to deplete the OSC, $M \in (13, 14)$, or to operate at stoichiometry, $M \in (12, 1)$. Alternatively, another switch to HCCI can be initiated if requested by R_{in}.

3. Supervisory control strategies

In this section two supervisory control strategies are discussed, described in detail in Nüesch and Stefanopoulou (2016). The two strategies are denoted *Baseline (Bsl)* and *Optimal Stay (Opt)* and in this paper they are responsible for the mode switching decision in the conventional vehicle and the mild HEV, respectively. The block diagrams of the two strategies are shown in Fig. 7.

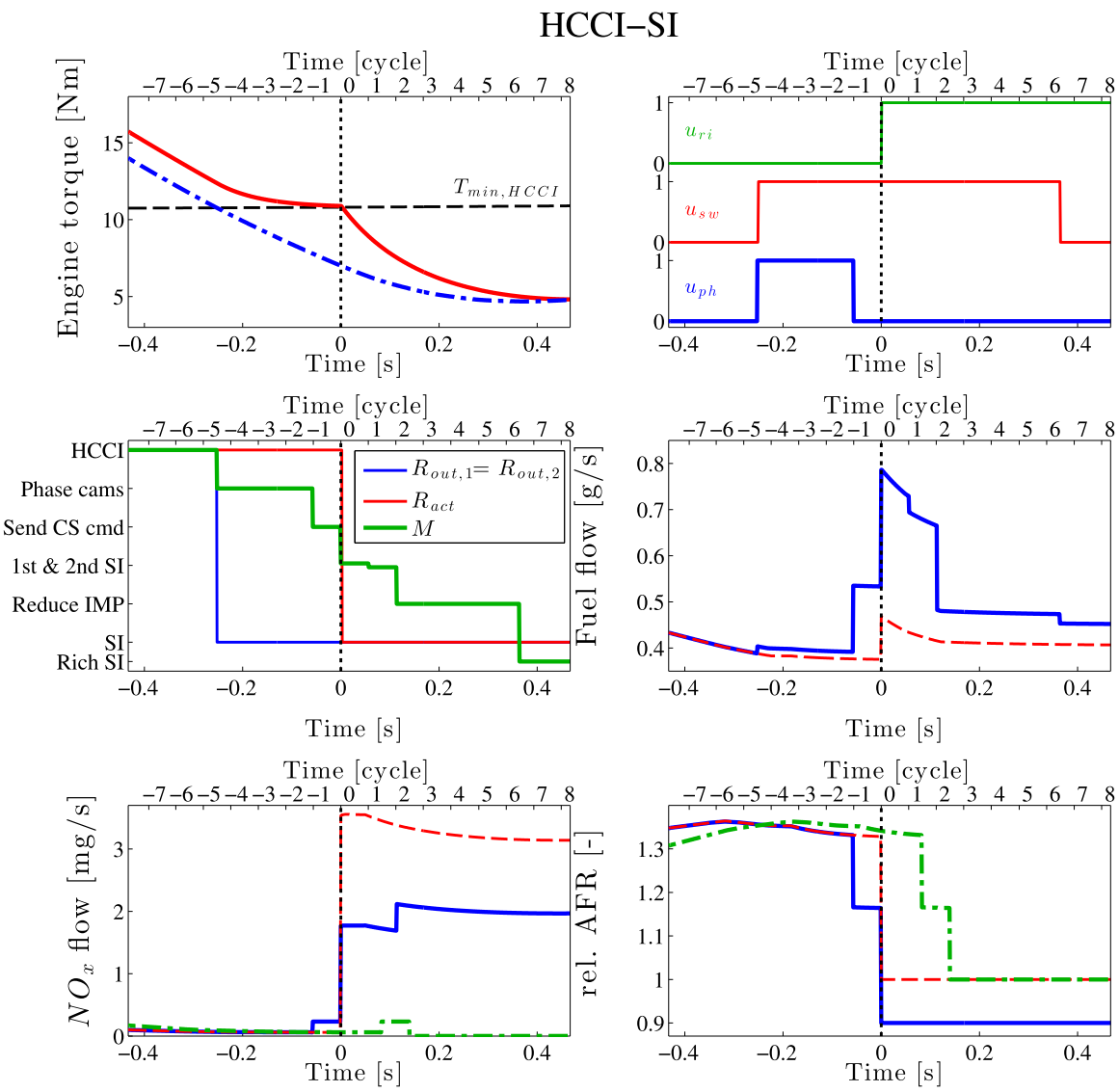

Fig. 6. Exemplary combustion mode switches from HCCI to SI during simulation of the conventional vehicle with supervisory strategy *Bsl* during the FTP75 drive cycle. The variables are plotted over time (bottom-axis) and engine cycles (top-axis). Engine speed is 2500 RPM.

3.1. Strategy 1: baseline (Bsl)

Supervisory strategy *Bsl* is applied here without any modifications compared to Nüesch and Stefanopoulou (2016).

3.2. Strategy 4: optimal stay (Opt)

An adjustment is made to strategy *Opt* to integrate the penalty from depleting the OSC into the ECMS-based mode switch decision. This adjust concerns the computation of the fuel power P_f:

$$P_f(\hat{T}_e, \hat{R}) = H_f \cdot \dot{m}_f(\hat{T}_e, \hat{R}, M) \tag{24}$$

$$\dot{m}_f(\hat{T}_e, \text{SI}, M) = \begin{cases} f_{SI}(\hat{T}_e, \omega_e) & M = \text{SI} \\ f_{SI}(\hat{T}_e, \omega_e)\cdot(1 + d_2) & M = \text{HCCI} \end{cases} \tag{25}$$

$$\dot{m}_f(\hat{T}_e, \text{HCCI}, M) = \begin{cases} f_{HCCI}(\hat{T}_e, \omega_e) & M = \text{HCCI} \\ f_{HCCI}(\hat{T}_e, \omega_e)\cdot(1 + d_1) + d_{ri} & M = \text{SI} \end{cases} \tag{26}$$

Besides total switching penalties d_1 and d_2, the supervisory controller also needs to take into account the additional fuel required to deplete the OSC after switching from HCCI to SI mode. For that reason the penalty d_{ri} is introduced. The value of d_{ri} is derived as follows: Based on Eq. (1) the total fuel mass spent during depletion the OSC $\widetilde{m}_{ri}$ can be estimated.

$$\widetilde{m}_{ri} = \frac{\Delta\widetilde{\Theta}\cdot\widetilde{C}_{0,1}\lambda_{14}}{0.23\cdot(1 + r_s\lambda_{14})(1 - \lambda_{14})} \tag{27}$$

with relative AFR λ_{14} during depletion in combustion mode M=14, $\lambda_{14} = 0.9$, fraction of the OSC to deplete $\Delta\widetilde{\Theta} = 0.9$, stoichiometric AFR r_s=14.7, and estimated OSC $\widetilde{C}_{0,1}$. The penalty for depleting the OSC in fuel flow can then be estimated using tuning parameter τ_2:

$$d_{ri} = \widetilde{m}_{ri}\cdot\frac{1 - \lambda_{14}}{\tau_2}. \tag{28}$$

The penalty shall only apply if $\widetilde{\Theta}$ is full. Therefore, together with (27) and (28):

$$d_{ri} = \begin{cases} \dfrac{\lambda_{14}\cdot\Delta\widetilde{\Theta}\cdot\widetilde{C}_{0,1}}{\tau_2\cdot 0.23\cdot 10^3\cdot(\lambda_{14}\cdot r_s + 1)} & \widetilde{\Theta} \geq 0.9 \\ 0 & \text{else.} \end{cases} \tag{29}$$

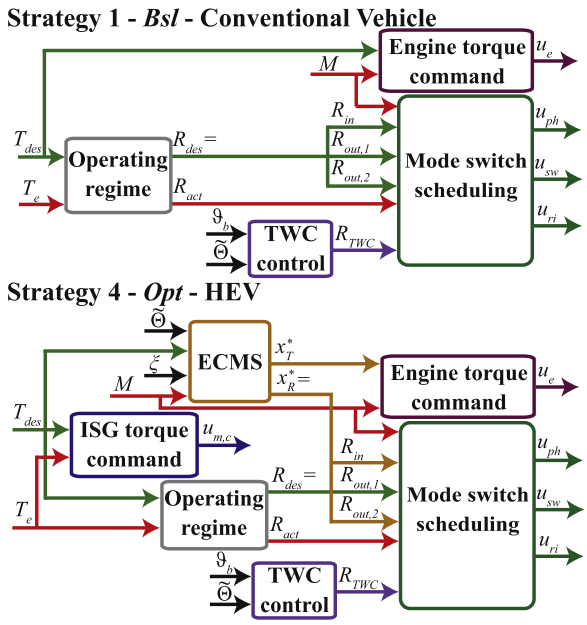

Fig. 7. Block diagrams of the two supervisory control strategies used in this paper.

4. Drive cycle results

In this section drive cycle results are analyzed to compare the performance of the two supervisory strategies. Also the differences are discussed between assuming an ideal aftertreatment system (Nüesch & Stefanopoulou, 2016) and a system consisting of two TWCs in series, requiring fuel-expensive depletion of the OSC.

Similar to the results in Nüesch and Stefanopoulou (2016) it is distinguished between instantaneous and penalized mode switches. For both cases it is assumed that the TWC's OSC does not exhibit any dynamics, i.e., it fills instantaneously when HCCI mode is entered and it returns to a depleted state as soon as stoichiometric SI is reached. Therefore these cases do not incur any fuel penalty from depletion. On the other hand, they also do not have the OSC to delay the NO_x breakthrough when entering HCCI. Note that the fuel economy results of those cases is the same as the corresponding cases in Nüesch and Stefanopoulou (2016). Finally, the last scenario includes OSC dynamics and depletion penalty.

4.1. Catalyst temperature

As mentioned before, subjecting the TWC to low HCCI exhaust gas temperature for extended periods of time can lead its to cool-down. This, in turn, would result in a decrease its conversion efficiency for *HC* and *CO* emissions. The trajectories of exhaust and brick temperatures during the simulation of the FTP75 drive cycle are therefore shown in Fig. 8. For both the conventional vehicle as well as the mild HEV three cases are compared: An SI-only engine and a multimode engine with and without OSC depletion.

As can be seen in Fig. 8, simulation suggests that in case of the conventional vehicle the impact of multimode combustion on exhaust temperature is relatively small, since residence time in HCCI mode is too short. Averaged over the course of the FTP drive cycle, this difference in temperature was computed to be around 11 °C. The consequence is a small difference in TWC brick temperature when comparing the SI-only case with the multimode one which assumes no OSC depletion. This average difference in brick temperature ended up being only 9 °C. However, simulation with the simplified TWC model shows that rich SI operation to deplete the OSC significantly increases the TWC temperature due to its oxidation of large amounts of *CO* and *HC* emissions. Therefore the TWC brick temperature for the case of SI/HCCI multimode combustion with OSC depletion is calculated to be in average 6 °C higher than the SI-only case. However, it needs to be noted that due to its simplicity the accuracy of the applied TWC model is expected to be below the above mentioned numerical values.

As can be seen for all cases, the mild HEV exhibits much lower temperatures than the conventional vehicle, in average 23 °C due to overall lower engine load. The mild HEV allows for significantly longer residence time in HCCI mode, resulting in an additional decrease in exhaust temperature of in average 27 °C, especially during 800–1000 s. This in turn translates into a drop in TWC brick temperatures of in average 15 °C. However, also in case of the HEV it can be seen that the requirement of running rich might counteracts and lead to a small temperature rise with brick temperature drop compared to SI-only of in average only 6 °C.

As can be seen, the use of the simple 0D-catalyst model does therefore not suggest a TWC temperature drop below light-off. For that reason, upon engine warm-up, the TWC's temperature did not act as a constraint. It follows that the conversion efficiencies for *HC* and *CO* were consistently high, deeming their breakthroughs irrelevant in this study. However, in reality it is possible that the spatial dynamics play a role. Specifically the front-end of the TWC is directly subjected to relatively cold HCCI exhaust gas. This in turn would result in an additional drop in temperature in this part of the catalyst and potentially lead to partial cool-down of the brick. Related simulation work by Kulzer et al. (2007) does show a significant reduction in TWC brick temperature and conversion efficiencies due to sustained operation in a low temperature combustion mode. Therefore, for more confidence on the subject of temperature-related interaction between low temperature combustion and TWC conversion efficiencies, additional and detailed modeling as well as more experimental data are required. In any case the control strategy suggested by Kulzer et al. (2007), can be applied to ensure high TWC temperature with only limited impact on fuel economy.

4.2. Fuel economy and NO_x emissions

The drive cycle results for fuel economy and tailpipe NO_x emissions are shown in Fig. 9. Note that, since results for the NO_x emissions are based on steady-state data, the absolute numbers need to be treated with caution and are in reality generally higher due to transient dynamics and imperfect AFR control.

The FTP75 drive cycle is subjected to engine and TWC cold start and therefore during the first 30 s the TWC's temperature lies below light-off, as can be seen in Fig. 8. This leads to the relatively high tailpipe NO_x results. However, upon reaching nominal temperatures the applied model assumes perfect AFR control and NO_x conversion in stoichiometric SI mode. For that reason NO_x in the SI-only cases during the HWFET and US06 cycles is equal to zero.

As can be seen for the FTP75 and the HWFET drive cycles, extended residence time in HCCI leads to long periods of NO_x breakthrough. The NO_x accumulates to significant amounts which would pose a problem for low emissions certification. Since during the US06 cycle HCCI combustion is even in the mild HEV only rarely used, the resulting NO_x emissions are relatively low.

Furthermore, the impact of the OSC dynamics can be seen clearly. For all the drive cycles and both vehicles the requirement of depleting the OSC leads to a significant drop in fuel economy. For the conventional vehicle the depletion overall negates all of HCCI's efficiency benefits. On the other hand, in case of the HEV and the FTP75 cycle still more than 2.5% improvement in fuel economy is achieved despite the OSC depletion. The important takeaway is twofold. First, hybridization does not lead to a noticeable improvement for the other drive cycles. Second, focusing on the NO_x emissions it can be seen that the buffer from the OSC does not lead to a significant reduction in tailpipe NO_x.

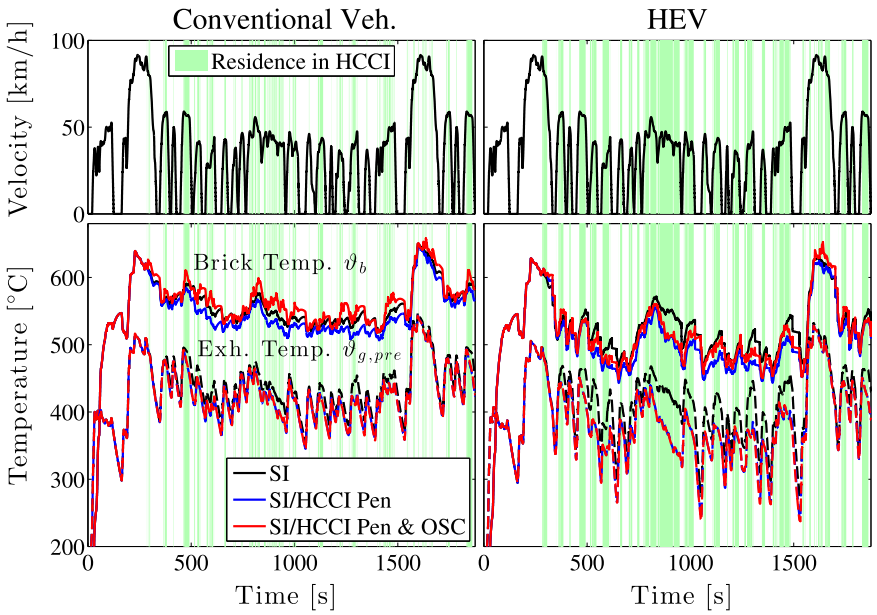

Fig. 8. Trajectories of the conventional vehicle (left) and the HEV (right) during the FTP75 drive cycle, periods in HCCI mode highlighted light green. Top: Velocity v; Bottom: TWC brick temperature ϑ_b (solid) and engine exhaust gas temperature $\vartheta_{g,pre}$ (dashed), SI-only (black), without OSC depletion (red), and with OSC depletion (blue). (For interpretation of the references to color in this figure legend, the reader is referred to the web version of this article.)

5. Case studies

The following section discusses two case studies which apply small modifications in HCCI-SI control strategy and hardware to the original mode switch parameterization *Org*. The results of the case studies and their impact on fuel economy and NO_x emissions are presented in Fig. 9 and denoted *Str* and *Sml*.

5.1. Case study 1: small HCCI regime with small OSC (Sml)

The first case study *Sml* discusses two hardware modifications. First, even if a TWC with generous OSC is used, this storage fills up too fast to lead to a substantial reduction in tailpipe NO_x, as can be seen in Fig. 9 when comparing the results of penalized mode switch with and without OSC dynamics. However, it requires a large quantities of fuel to deplete the full OSC. Therefore the usage of a TWC with a small rather than a large OSC might actually be desirable, thereby assuming that in SI-combustion AFR-control is accurate enough.

Second, it can be seen that extended operation in HCCI mode results in significant amounts of tailpipe NO_x, since the TWC's OSC is full for a substantial amount of time. In case of the HEV this effect is even enhanced. However, as shown in Fig. 3, while HCCI engine-out NO_x is very low at the bottom half, it reaches significant values towards higher loads. At the same the engine often operates at those higher loads, as seen in Nüesch and Stefanopoulou (2016). This is especially true in case of the HEV when the driver desires a torque higher than the maximum HCCI load while the ISG compensates for the difference. Finally, as also seen in Fig. 3, efficiency benefits from using HCCI compared to SI at these higher loads are relatively small.

Therefore simulations were run, assuming only the lower half of the HCCI regime (in Fig. 3 area below purple dashed line) combined with a TWC with a quarter of the original OSC. The associated results are shown in Fig. 9 marked with Supervisors *Bsl/Sml* and *Opt/Sml*. As can be seen the fuel economy of this modified configuration is almost equal or greater than the original results. In addition, tailpipe NO_x originating from HCCI operation is significantly reduced.

5.2. Case study 2: stratified HCCI-SI switch (Str)

The second case study *Str* discusses a potential variation in the HCCI-SI mode switch control strategy. As discussed in Section 2.2.1 the original control strategy attempts rich SI operation from right after the cam switch to high lift. The goal of this procedure is to enable the TWC to convert SI combustion's high levels of engine-out NO_x as fast as possible to avoid break-throughs. The downside of this strategy, however, is a substantial fuel penalty during the first two SI engine cycles. As a direct consequence this results in a trade-off between fuel economy and NO_x emissions. In this case study an alternative strategy is tested, in which the first two engine cycles after the cam switch are run in stratified lean SI combustion, comparable to the mode switch strategy presented by Tian, Ge, Wang, and Shuai (2007). In this case the correct amount of fuel is injected to match the torque request while not constraining AFR in SI mode. Detailed HCCI-SI mode switch simulations of this strategy have shown a relative AFR of approximately $\lambda = 1.7$ during the first and $\lambda = 1.2$ during the second SI cycle. Fuel penalties of 1.07 and 1.06 were assumed. Include NO_x assumption. It is assumed that after those two lean SI cycles the engine can be operated either at stoichiometry or rich, if the OSC needs to be depleted. The original and modified parameters can be found in Table 3. An exemplary HCCI-SI mode switch is shown in Fig. 10 to compare this parameterization with the original one.

The results are shown in Fig. 9, denoted as *Bsl/Str* and *Opt/Str* for the conventional vehicle and the HEV, respectively. As can be seen for both vehicle configurations as well as all three drive cycles, the resulting improvements in fuel economy are almost negligible, while the tailpipe NO_x emissions, however, are noticeably increased.

6. Conclusion

A drive cycle model of a mild HEV with SI/HCCI multimode engine and TWC aftertreatment is discussed in terms of fuel economy and NO_x emissions. ECMS is applied to not only determine an optimal torque split between the multimode engine and ISG but also the desired combustion mode. The control strategy takes into account fuel penalties associated with mode switching and OSC depletion. The ISG's torque assist allows for extended residence time in HCCI mode, thereby reducing the amount of fuel needed on depleting the OSC. However, this prolonged operation under lean conditions results in extended periods of time under which the TWC is unable to reduce NO_x, leading to substantial tailpipe emissions.

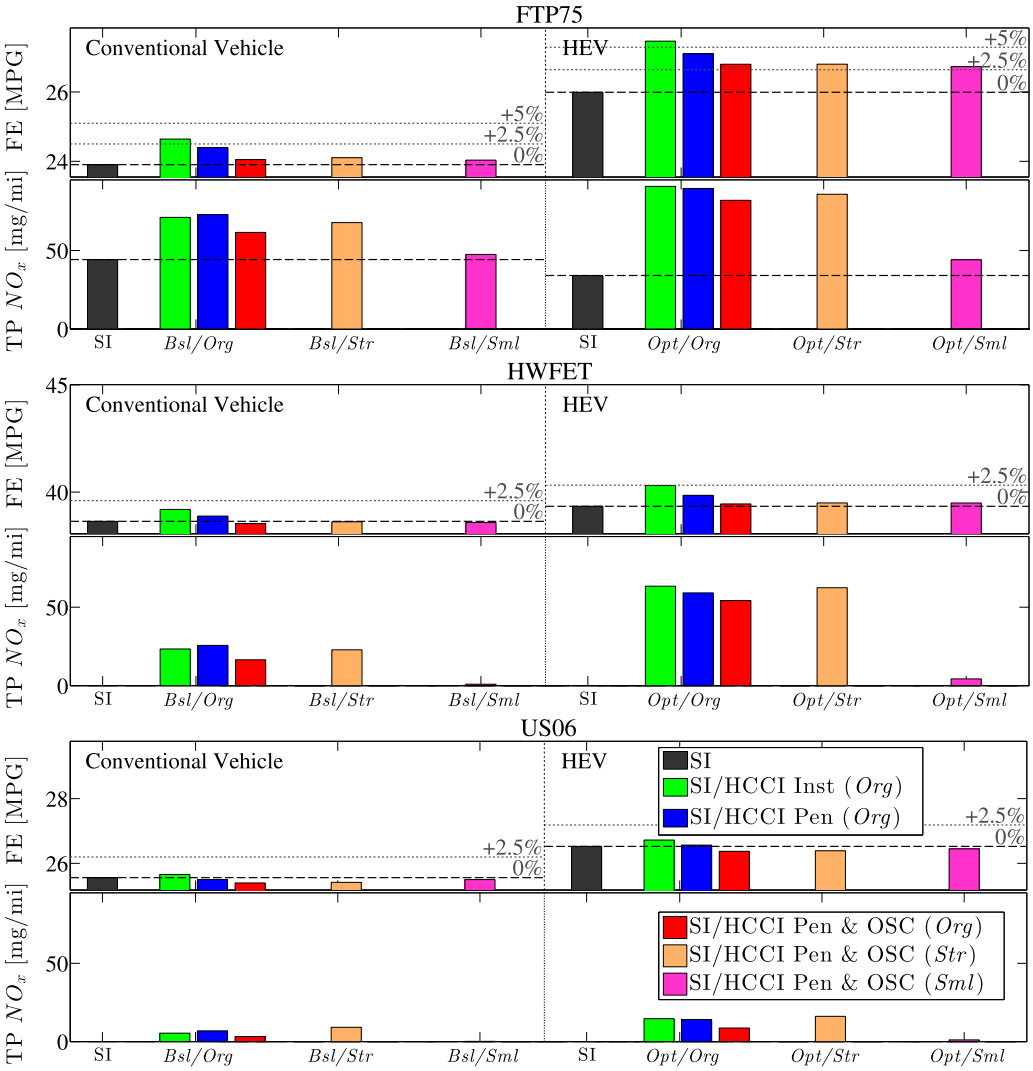

Fig. 9. Drive cycle results assuming a TWC, which requires OSC depletion. Results for FTP75 (top), HWFET (middle), and US06 (bottom) cycles. Plotted are fuel economy (upper) and average tailpipe NO_x (lower). Conventional vehicle (bars on the left) and mild HEV (bars on the right) with results shown for the SI-only engine (black bars) as well as the SI/HCCI multimode engine applying the supervisory strategies *Bsl* and *Opt*. Mode switches are assumed instantaneous (green bars), penalized (blue bars), and penalized with OSC depletion (red bars). Results from the original mode switch model are denoted *Org*. Also shown are results for case study *Str* with modified HCCI-SI mode switch and case study *Sml* with reduced OSC capacity and HCCI regime. (For interpretation of the references to color in this figure legend, the reader is referred to the web version of this article.)

Table 3
Modified mode switch model parameters for case study *Str*.

	State M	FP d_M	Δt_M	λ_M	$NO_{x,M}$
Org	10 (SI)	68%	1 cyc	0.9	$0.5NO_{x,SI}$
	11 (SI)	60%	1 cyc	0.9	$0.5NO_{x,SI}$
Sml	10 (SI)	7%	1 cyc	1.7	$0.8NO_{x,SI}$
	11 (SI)	6%	1 cyc	1.2	$0.9NO_{x,SI}$

A simple 0D-temperature model for the TWC was used to also account for the influence of temperature on conversion efficiency. Based on this simple model operation in HCCI mode did not lead to a significant drop in TWC brick temperature compared to the HEV with SI-only engine. In fact, running the engine rich to deplete the OSC lead to exothermic reactions which partially compensated for the cold HCCI exhaust gas. However, experiments and additional work with detailed TWC simulations are needed to confirm this statement.

Finally, in the end of the paper two case studies are presented. The first study discusses the combined sizing of the TWC's OSC and the regime where HCCI combustion is feasible. Under lean HCCI conditions even a generous OSC fully oxidizes rapidly and is therefore unable to maintain significant conversion of NO_x emissions. This study suggests that it is preferable to reduce the size of the OSC to decrease the amount of fuel required for its depletion. In terms of HCCI regime it can be seen that the push to a higher load limit correlates with increasing combustion temperatures and engine-out NO_x emissions. Therefore, constraining the HCCI regime to lower load conditions, exhibiting ultra-low NO_x emissions, substantially reduces the associated breakthrough. It is seen that even a smaller HCCI regime can be utilized for significant periods of time by leveraging the ISG's torque assist. Furthermore, the fuel savings originating from the smaller OSC compensate for the reduced HCCI residence time.

In the second study, based on assumptions, the parameterization of the mode switch model is modified to describe a HCCI-SI switch under stratified instead of stoichiometric or rich SI conditions. While applying stratification reduces the fuel penalty of the HCCI-SI mode switch it also rises tailpipe NO_x emissions. Based on the assumed parameters it is shown that over the course of a drive cycle this strategy can lead to a substantial increase in NO_x while the fuel economy remains virtually the unchanged.

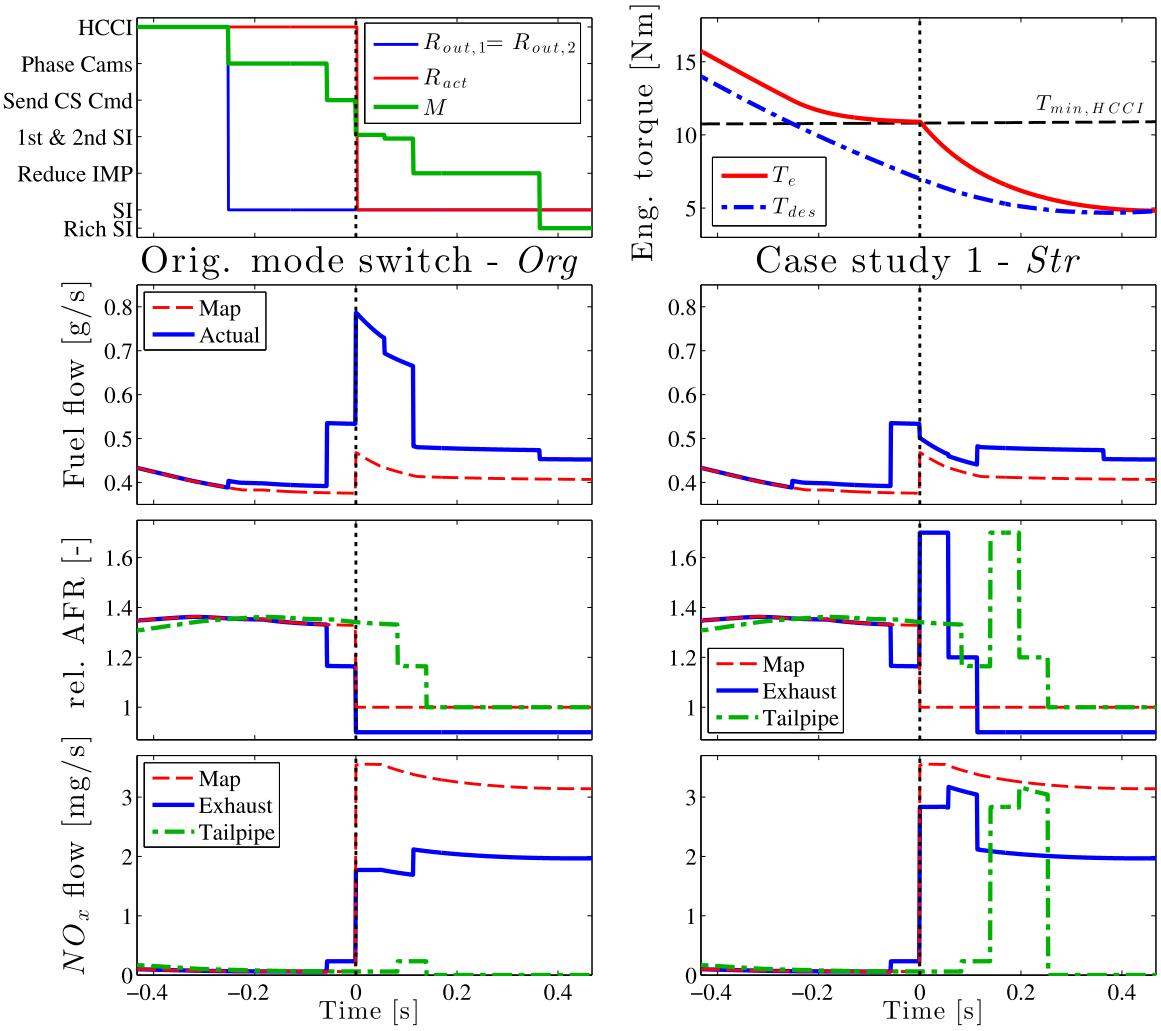

Fig. 10. Exemplary HCCI-SI mode switch as in Fig. 6. Lower six plots to compare the original (left) with the parameterization of case study 1 (right).

Acknowledgements

The authors wish to thank Drs. John Hoard and Galen Fisher for helpful discussions about TWC aftertreatment.

References

Brandt, E., Wang, Y., & Grizzle, J. (2010). Dynamic modeling of a three-way catalyst for SI engine exhaust emission control. *IEEE Transactions on Control System Technology*, 8(5), 767–776.

Chen, Y., Sima, V., Lin, W., Sterniak, J., & Bohac, S. (2015). Lean HCCI/rich SACI gasoline combustion cycling and three-way catalyst for fuel efficiency and NOx reduction. *Journal of Engineering for Gas Turbines and Power*, 137(12), 121508-1–121508-7.

Gao, Z., Conklin, J., Daw, C., & Chakravarthy, V. (2010). A proposed methodology for estimating transient engine-out temperature and emissions from steady-state maps. *International Journal of Engine Research*, 11, 137–151.

Gorzelic, P. (2015). Modeling and model-based control of multi-mode combustion engines for closed-loop SI/HCCI mode transitions with cam switching strategies. (Ph.D. thesis), University of Michigan.

Guzzella, L., & Onder, C. (2010). *Introduction to modeling and control of internal combustion engine systems* Berlin Heidelberg: Springer-Verlag.

Heywood, J. B. (1988). *Internal combustion engine fundamentals* New York: McGraw-Hill Education.

Kibitz, P., Onder, C., & Guzzella, L. (2012). Control-oriented modeling of a three-way catalytic converter with observation of the relative oxygen level profile. *Journal of Process Control*, 22, 984–994.

Kiwitz P. (2012). Model-based control of catalytic converters, (Ph.D. thesis), ETH Zurich.

Kulzer, A., Hathout J. -P., Sauer, C., Karrelmeyer, R., Fischer, W., & Christ A. (2007). Multi-mode combustion strategies with CAI for a GDI engine. In *SAE*, no. 2007-01-0214.

Kum, D., Peng, H., & Kucknor, N. K. (2011). Supervisory control of parallel hybrid electric vehicles for fuel and emissions reduction. *Journal of Dynamic Systems, Measurement, and Control*, 133, 061010-1–061010-10.

Nüesch, S., Jiang, L., Sterniak, J., & Stefanopoulou, A. (2015). Fuel economy of a multimode combustion engine with three-way catalytic converter. *Journal of Dynamic Systems, Measurement Control*, 137, 051007-1–051007-10.

Nüesch, S. (2015). Analysis and control of multimode combustion switching sequence. (Ph.D. thesis), *University of Michigan*.

Nüesch, S., & Stefanopoulou A. (2016). Mild HEV with multimode combustion: Benefits of a small oxygen storage. In *IFAC AAC*.

Nüesch, S., & Stefanopoulou, A. (2015). Is it economical to ignore the driver? A case study on multimode combustion. In *ASME DSCC*.

Nüesch, S., & Stefanopoulou, A. (2016). Multimode combustion in a mild hybrid electric vehicle. Part 1: Supervisory control. *IFAC Control Engineering Practice*.

Nüesch, S., Gorzelic, P., Jiang, L., Sterniak, J., & Stefanopoulou, A. (2016). Accounting for combustion mode switch dynamics and fuel penalties in drive cycle fuel economy. *International J. Eng. Res.*

Sanketi, P. R., Hedrick, J. K., & Kaga T. (2005). A simplified catalytic converter model for automotive coldstart control applications. In *Proceedings of ASME IMECE*.

Shaw, B. T., Fischer, G. D., & Hedrick, J. K. (2002). A simplified coldstart catalyst thermal model to reduce hydrocarbon emissions. In *Proceedings of IFAC 15th Triennial World Congress*.

Tian, G., Ge, Q., Wang, J., & Shuai, S. (2007). Control of a spark ignition homogeneous charge compression ignition mode transition on a gasoline direct injection engine. *Proceedings of Institution of Mechanical Engineers Part D: Journal of Automobile Engineering*, 221, 867–875.